ELSEVIER

Contents lists available at ScienceDirect

Soil Dynamics and Earthquake Engineering

journal homepage: http://www.elsevier.com/locate/soildyn





Experimental study on wave isolation performance of periodic barriers

Hsuan Wen Huang ^a, Benchen Zhang ^b, Jiaji Wang ^{a,*}, F.-Y. Menq ^b, Kalyana Babu Nakshatrala ^a, Y.L. Mo ^a, K.H. Stokoe ^b

- a University of Houston, Houston, TX, USA
- ^b The University of Texas at Austin, Austin, TX, USA

ARTICLE INFO

Keywords:
Periodic barrier
Metamaterial
Field test
Excitation direction
Frequency band gap
Shake truck

ABSTRACT

A wave barrier—combining the advantages of trench-type wave barriers and metamaterials—is made by infilling the trench-type wave barrier with metamaterials. In this research, a series of full-scale field experiments are conducted to investigate the screening effectiveness of both empty trench and periodic barriers. The precast unit cells of periodic barriers are arranged to form one long barrier with a length of 2.44 m, one short barrier with a length of 1.22 m, or two short barriers with a length of 1.22 m to examine the influence of barrier length and the number of unit cells on the wave isolation performance. The state-of-the-art high-force triaxial (T-Rex) shaker truck is used to generate excitation in the vertical, horizontal inline, and horizontal crossline directions. Three excitation inputs are tested, including fix-frequency harmonic excitations, frequency sweeping excitations, and the earthquake excitation. For each test, a benchmark test is conducted prior to the barrier installation. The ground surface responses at each geophone location are recorded in all three directions. The normalized response of each point, the responses in front of the barrier and behind the barrier, and the frequency response function (FRF) are presented in detail. Test results show that the various excitation inputs lead to similar results. The performance of the periodic barrier is found to depend on the excitation directions due to the dominate wave form. By comparing the FRF between the benchmark case and the case with periodic barriers, the screening effectiveness of periodic barriers can be identified in some frequency ranges, which are expected to be the frequency band gaps of the periodic barriers.

1. Introduction

The wave barrier is a typical measure to isolate the vibration transmitted on the surface to the protected structure by introducing the discontinuity on the path of wave propagation. Wave barriers can be classified into active and passive barriers, depending on the distance between the vibration source and the wave barrier. The barriers installed in the vicinity of the vibration source are classified as active isolation barriers [1,2]. The barriers installed close to the protected structures are classified as passive isolation barriers [3,4]. This study aims to study the performance of the periodic barrier as the passive isolation barrier. The typical form of wave barrier is the empty trench or infilled trench wave barrier. Studies indicate that open trenches are more efficient than infilled trenches. Woods [5] conducted a series of full-scale field tests to investigate the screening effectiveness of the trench barrier under the vertical vibration for both active and passive

isolation barriers and proposed design recommendations for the empty trench barrier. However, the instability of the empty trench makes the infilled trench wave barrier a common practice. To investigate the influence of geometry and the material properties on the effectiveness of the infilled trench-type wave barrier under the vertical excitation, small-scale lab experiments [6,7], and large-scale field tests [5,8–11] were conducted by various researchers. The barrier depth is considered the most important geometry property of the wave barrier. The normalized depth (defined by the physical depth of the barrier divided by the Rayleigh wavelength of soil) equal or above 0.6 is recommended. The infilled material of the wave barrier is classified by its Young's modulus. If Young's modulus of the infilled material is greater than the soil, the infilled wave barrier is called the stiff barrier. On the other hand, if Young's modulus of the infilled material is smaller than the soil, the infilled wave barrier is called the soft barrier. The experiments have shown that either stiff wave barriers or soft barriers can mitigate the

E-mail addresses: hhuang15@uh.edu (H.W. Huang), thebens@utexas.edu (B. Zhang), jwang215@central.uh.edu (J. Wang), fymenq@utexas.edu (F.-Y. Menq), knakshatrala@uh.edu (K.B. Nakshatrala), yilungmo@central.uh.edu (Y.L. Mo), k.stokoe@mail.utexas.edu (K.H. Stokoe).

^{*} Corresponding author.

vertical ground vibration. Along with the geometry and the material properties of the wave barriers, the frequency-dependent screening effectiveness is recognized. Other than the above-mentioned parameters, the loading distance, which is defined by the distance between vibration and the wave barrier, and the number of the barriers are found influential to the performance of the barrier system. However, not only the effect of excitation direction but also the response in different direction are in absence of most of the available experimental program. In present study, the excitations in all three direction are applied on the ground surface and the ground surface responses in all three direction are recorded.

A new type of seismic isolation barrier called "periodic barrier," which combines a trench-type wave barrier and a metamaterial, is investigated in this research. The metamaterial is made of repetitive composite unit cells, which possess a unique frequency-selective property to manipulate how stress waves propagate through the material [12-14]. When the exciting frequency lies within a certain frequency range (frequency band gap), the vibration, sound, and phonons will be forbidden. With the proper design of metamaterial, the frequency band gaps can be manipulated to serve the desired purpose. By infilling the metamaterials in the trench-type wave barrier, the periodic barrier combines the advantages of both the wave barrier and the metamaterials. The metamaterial has been adopted in the foundation isolation, small-scale lab experiments [15], large-scale shake table tests [16-18], or large-scale field test [19,20] were conducted to demonstrate the feasibility of using the metamaterial to provide the vibration isolation. While the foundation isolation is directly attached to the building, which inevitably poses several disadvantages such as large deformation and difficulty in maintained, the periodic barriers are completely detached to the protected building, so the disadvantages of the foundation isolation are overcome by the periodic barrier. The periodic barriers are studied by various researchers in many different forms, such as boreholes [21-25], cylindrical tubes [26,27] or rectangular prism [28] containing a resonator, infilled trench [23].

The periodic barrier in this study is the trench type wave barrier infilled with metamaterial comprising reinforced concrete (RC) and polyurethane layers. By burying around the protected area, the periodic barrier can block incoming waves within the frequency band gaps and thus mitigate damages due to seismic activities. To stress the importance of the excitation direction and exciting frequency on the periodic barrier's performance, in this research, the state-of-the-art high-force triaxial (T-Rex) shaker truck is used to generate excitation in the vertical, horizontal inline, and horizontal crossline directions, and the exciting frequencies ranging from 15 Hz to 100 Hz are used. Moreover, the ground surface response has been recorded in all three directions within an extended region shielded by the periodic barrier.

The rest of the paper is organized as follows. We first illustrate the experiment program, including the design and manufacture of the specimens, experiment layout, test procedure, and the strategy of interpreting raw data to quantify the performance of the barrier. Next, the experimental response of the soil and the screening effectiveness of the periodic barrier are reported.

2. Experimental program

2.1. Dispersion relation of the periodic barrier

The periodic barrier is made of the unit cell that has 3 layers constituents including the concrete and polyurethane materials. The 3-layer-unit-cell 1D metamaterial is illustrated by Huang et al. [13]. The properties of polyurethane were tested and reported by Witarto [29]. Since the same batch of the polyurethane pads are used in our test, the properties of the polyurethane pads are the same as reported by Witarto [29]. For concrete layer, the compression test on concrete cylinder was conducted according to ASTM standard, and its Young's modulus is obtained through ACI code. The first and the third layers (RC): $E_1 =$

30.44 GPa, $\rho_1 = 2400 \text{ kg/m}^3$, $\nu_1 = 0.2$, $h_1 = 101.6 \text{ mm}$. The second layer (polyurethane): $E_2 = 0.1586$ MPa, $\rho_2 = 1100$ kg/m³, $\nu_2 = 0.463$, $h_2 = 0.463$ 76.2 mm [13]. Huang et al. [13] also reported the dispersion relation of this 3-layer periodic barrier. The dispersion relation relates the frequency to the corresponding real wave number. The frequency band gap of the metamaterial can be identified in the dispersion relation where the corresponding wavenumber is in complex form. When the exciting frequency lies within its frequency band gaps, the wave propagation will be prohibited. The resulting theoretical frequency band gaps within the range from 0 to 100 Hz for the unit cell are found below. For the P wave, the theoretical frequency band gap is 45.0-100 Hz; for the S wave, the theoretical frequency band gaps are 11.8-46.1 Hz, 49.1-92.1 Hz and 93.7-100 Hz; for the Rayleigh wave, the band gaps are 10.2-43.8 Hz, 47.0-87.6 Hz, and 88.8-100 Hz [13]. The frequency band gaps of the 1D metamaterial are desgined to fall within 10-100 Hz due to the optimal frequency range of the triaxial shake truck (T-Rex) used in the experimental program [30].

2.2. Fabrication of periodic barriers

Fig. 1 shows the assembly of the periodic barrier in this research. A unit cell of the periodic barrier consists of two reinforced concrete (RC) layers and one polyurethane layer. The dimension of each RC layer is 1.52 m long, 1.22 m wide, and 0.1 m thick. One layer of #4 rebar (13 mm diameter) layouts with 0.13 m (5 inches) separation in both the longitudinal and transverse directions is used for the RC layer. The yield stress of the rebars is 413.7 MPa. The periodic barrier was precast in the lab for better quality control to prevent the formation of honeycombs inside the RC layers. After the surface was clean and smooth, the polyurethane pads were pasted on top of the RC layers using high strength epoxy, and the sides of the polyurethane pads were sealed with polyurethane-based sealant. After the epoxy was cured, the weights were removed, and the remaining RC layers were pasted on top of the polyurethane layers using epoxy as shown in Fig. 1.

2.3. Test setup

Fig. 2 shows the schematic diagrams for each barrier condition. A total of five conditions are investigated in this research. First, a benchmark test (denoted as S0) is conducted prior to the barrier installation. Second, a long empty trench (denoted as EL) with a length of 2.44 m, a depth of 1.52 m, and a width of 0.28 m is studied. Subsequently, a long periodic barrier (denoted as BL) with a length of 2.44 m, a depth of 1.52 m, and a width of 0.28 m is studied. A short periodic barrier (denoted as B1) with a length of 1.22 m, and a width of 0.28 m is studied. Finally, two short periodic barriers (denoted as B2) are separated by 2.6 m apart due to the construction difficulty. Each short periodic barrier has the dimension of 1.22 m long, 1.52 m deep, and 0.28 m wide. When calculating the frequency band gaps of the periodic barrier, the soil is not considered as part of the material due to its inhomogeneity.

The barrier placed 6.1 m away from the vibration source is used to shield the structure located 1.4 m behind the barrier location. Deployed along the line perpendicular to the length direction of the barrier fifteen





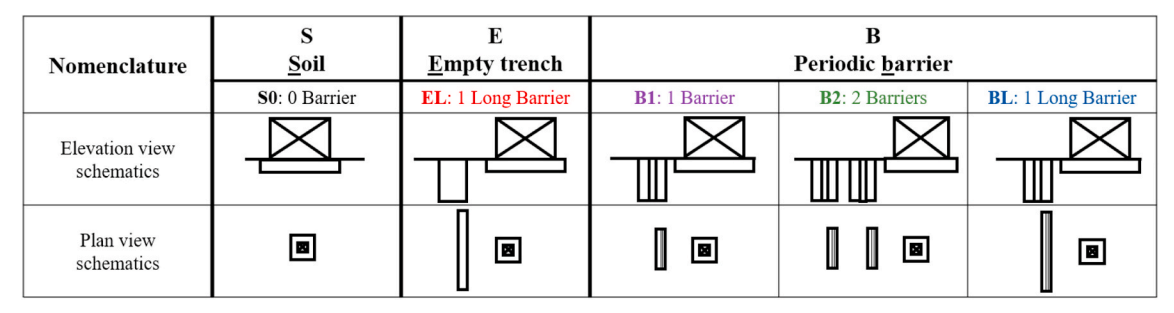


Fig. 2. Schematic diagram and nomenclature (not to scale).

3-D geophone stations are installed on the ground surface to monitor the ground motions. Each geophone station contains of one vertical and two horizontal geophones (GS-One LF 4.5 Hz). The layout of sensors, structure, periodic barrier, and the loading point is illustrated in Fig. 3 and the test photos are shown in Figure 4. As shown in Fig. 4, the vertical direction is defined to be perpendicular to the ground surface, the horizontal inline direction is the direction that coincides with the line connecting the vibration source to the center of the structure, and the horizontal crossline direction is perpendicular to both the horizontal inline and vertical direction. The responses in the vertical, horizontal inline, and horizontal crossline directions are recorded at each sensor location.

For each of the barrier conditions, three different excitation input signals: 1) fix-frequency harmonic excitations, 2) frequency sweeping excitations, and 3) earthquake excitations, are applied in all three directions to study the dynamic behavior of soil due to the installation of barriers. First, the signal with constant frequency and amplitude is used in fix-frequency harmonic excitation. With a duration of 2 s for each exciting frequency, the fix-frequency harmonic excitation uses the 18 frequencies ranging from 15 Hz to 100 Hz with a 5 Hz interval. The advantage of the fix-frequency harmonic excitation is the high signal-tonoise ratio due to its concentrated energy at individual frequency. Second, the signal for the frequency sweeping excitation sweeps through 100 Hz-15 Hz within a duration of 12 s. The advantage of frequency sweeping excitation is to obtain the dynamic behavior within the frequency range of interest in a fairly short time. Third, nine earthquake seismograms include Oroville, Anza, Bishop, Loma Prieta, TCU052, Gilroy, San Fernando, El Centro, and Northridge are provided as the input signals. The original time-histories are obtained from PEER ground motion database. The optimum performance of T-Rex is between 10 and 100 Hz. To match this frequency range, the time axis of each of the seismograms is scaled by multiplying with a scale factor so that its main frequency content is also within 10-100 Hz. The scale factors for all seismograms are listed in Table 1. The advantage of using the earthquake seismograms as the input signal is to obtain the dynamic behavior of the soil and structure under the earthquake excitation. The excitation is applied in all three directions, and the response in the same direction as the excitation direction is used to evaluate the performance of the barrier.

The function generator (Keysight technologies Inc. Model: 33512B) shown in Fig. 5 is capable of creating a simple waveform for the drive source signals to control the shaker truck, T-Rex. For the complex waveform such as the signals for earthquake excitation, those

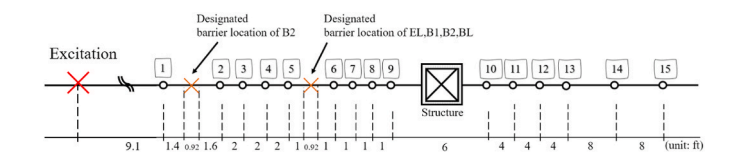


Fig. 3. Experiment layout (not to scale; $1\ \mathrm{ft}=0.3\ \mathrm{m}$), each geophone station is numbered in the figure.

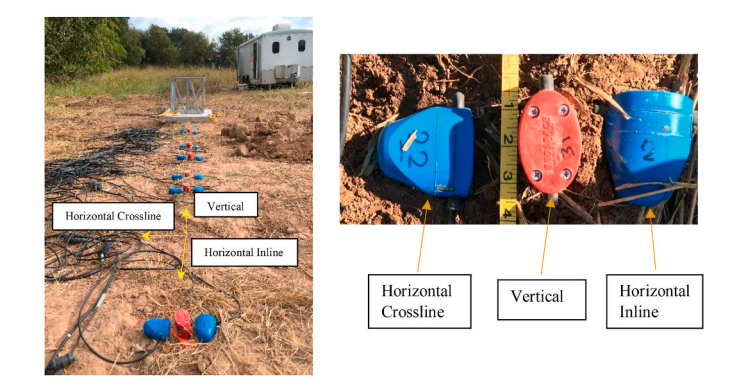


Fig. 4. 3D geophones deployment.

Table 1Scale factors of the earthquake input signals.

Earthquake events	Scale factor
Oroville	0.14
Anza	0.14
Bishop	0.17
Loma Prieta	0.03
TCU052	0.01
Gilroy	0.11
San Fernando	0.05
El Centro	0.025
Northridge	0.025

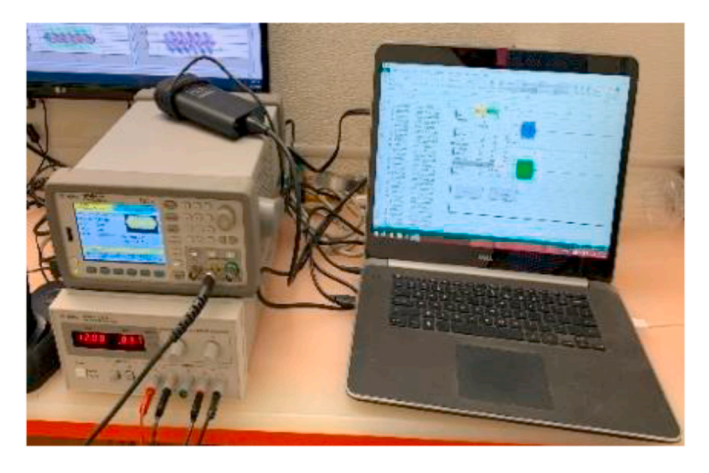


Fig. 5. Function generator.

deliberately manipulated signals can be generated from the excel sheet and sent to the function generator. Connected to the shaker, the function generator can send the signals to the shaker and trigger the shaker to generate the vibration with desired waveform. The geophones are connected to a dynamic signal analyzer from Data Physics Inc. called the Mobilyzer. As shown in Fig. 6, several Mobilyzers can be connected to provide large number of channels for all the sensors. As shown in Fig. 7, the signals collected from the sensors are displayed in a monitor in real-time.

The test starts with marking the position of the structure, sensors, and shaker location. After the preselected positions are marked, the shaker and structure are moved to the designated position, and geophones are installed for all three directions at each sensor location. Geophones are leveled during installation and all the sensors are calibrated before the test. Prior to the installation of the barrier, the benchmark case, S0, is tested first. Shaker T-Rex can generate large dynamic forces in three directions. These directions are vertical, horizontal crossline, and horizontal inline directions. Different excitation directions are applied on the ground surface to simulate different dominated wave types and to study the performance of the barrier under different types of waves. Rayleigh wave, Love wave, and P wave are the dominated wave types for the excitation applied in the vertical, horizontal crossline, and horizontal inline directions, respectively. Shown in Fig. 8, a 2.44 m long, 1.52 m deep, 0.28 m wide empty trench is excavated at the designated barrier location for the barrier condition EL. After completing the test on the case EL, the precast periodic barrier is placed into the empty trench for the barrier condition of BL shown in Fig. 9. Finally, two 1.22 m long, 1.52 m deep, 0.28 m wide periodic barriers are placed. The two periodic barriers are placed 2.6 m apart from each other. A typical passive isolation test setup with steel frame structure is shown in Fig. 10. As shwon in Fig. 10, the overall dimension of the steel frame is $0.6m \times 0.6m \times 0.6m$ to simulate a single-storey steel structure. The steel frame is assembled using slotted steel angle members (Everbilt 1-1/2 in. x 14-Gauge x 72 in. Zinc-Plated Slotted Angle). The cold-rolled steel material is coated with Zinc coating. The cross section has leg length of 38.1 mm and plate thickness of 2.0 mm. Holes were bored on the section to facilitate connection of steel frame by the manufacture. The steel frame is connected using bolts. In addition, two 6 mm steel plates of 18.6 kg weight are applied on top and bottom of the steel frame.

The data collected from the sensor is first converted to either velocity according to the calibration factor of the sensors. The velocity reading is later converted to acceleration by taking a derivative with respect to time. Before analyzing the data, the Tukey window, which is a cosine-tapered window with the cosine fraction of 0.12, was used to make the signal outside the recording duration zero. After windowing the signal, a 5th order low-pass, high-pass Butterworth filter, which is an anti-aliasing filter, was applied to the recording. To eliminate the response at the natural frequency of the geophones, since the natural

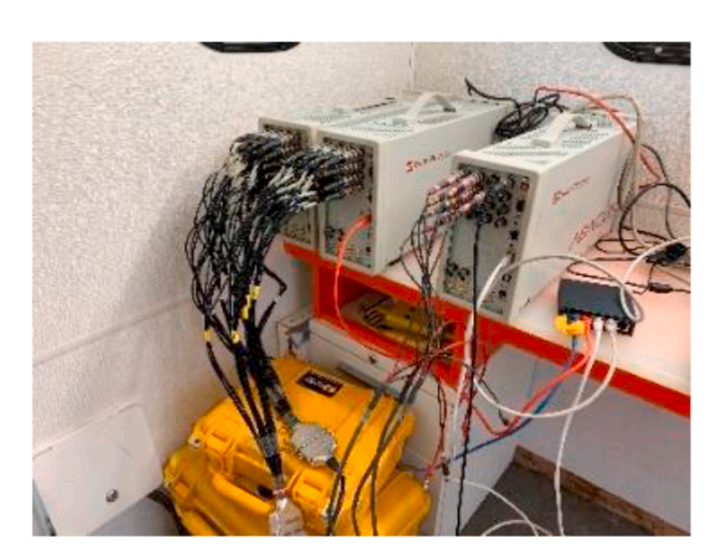


Fig. 6. Data acquisition system.

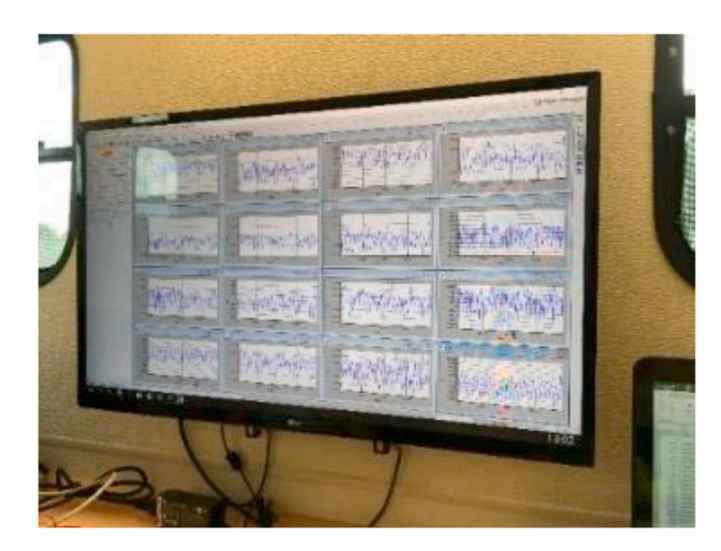


Fig. 7. Real-time monitoring.



Fig. 8. Empty trench excavation.

frequency of the geophone is 4.5 Hz, the low-pass cut off frequency is set to 5 Hz to attenuate the signal below 5 Hz. The processed data is used for evaluating the performance of the barrier by following the definition in Sect. 2.5.

2.4. Shear wave velocity profile of soil

The Spectral-Analysis-of-Surface-Waves (SASW) testing is conducted to determine the shear wave velocity profile. The SASW test method utilizes the dispersive nature of Rayleigh-type surface waves propagating through a layered material to determine the shear wave velocity profile of the material (Stokoe et al., 1994). The SASW testing array is parallel to the sensor array installed for the periodic barrier testing with a spacing of approximately 2.5 m. The dispersion curves obtained from the SASW testing in both forward and reverse directions is shown in Fig. 11(a). As shown in the figure, there is no clear difference between the dispersion curves from the forward direction and the those from the reverse direction. A compacted (averaged) dispersion curve is derived from all experimental dispersion curves with a 4th order polynomial fitting procedure. The theoretical dispersion curve that is considered to best match the compacted experimental dispersion curve is developed by iteratively changing the thickness and shear wave velocity of each



Fig. 9. Barrier installation.

layer in the shear wave velocity profile. The shear wave velocity profile that generates the best-fit, theoretical dispersion curve in Fig. 11(a) is shown in Fig. 11(b). The maximum depth to which the shear wave velocity profile was determined is $\lambda_{max}/2$ or 6 m.

2.5. Definition of frequency response function

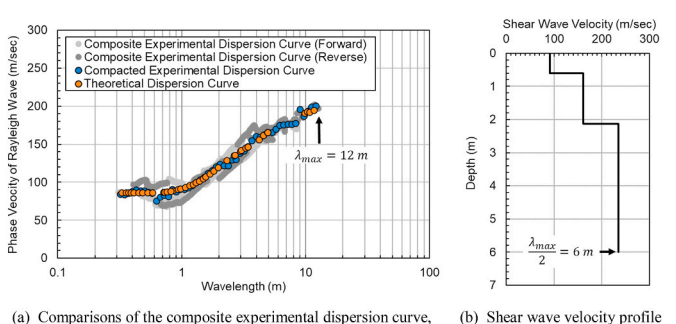
The screening effectiveness of the periodic barrier is quantified by the Frequency Response Function (FRF) and the response in the same direction as the excitation direction is used to evaluate the performance of the barrier. Two different methods are used to calculate the FRF: "Direct method" and "Average method". Direct method takes the responses of nearest points in the front and the back of the barriers to calculate the FRF; Average method takes the responses of several points behind the barriers and incorporates the response in benchmark case to calculate the FRF. Due to the limitation of the shaker to generate the exact same vibrations when receiving the same input signal, normalized responses is required when adapting Average method to compare between different barrier condition with the benchmark cases. The response is normalized based on the response at the reference point which is nearest point in front of the barriers. While there is no such requirement to normalize the response for Direct method because the response for each barrier conditions are considered separately.

Different approach is used to process the data based on the form of the input signal. When the fix-frequency harmonic excitation is applied, it is found that the signal will have the spikes before it reaches a steady response. After excluding those spikes, the maximum steady-state response can be extracted at each recording point for every exciting frequency.

Eq. (1) shows the expression to calculated FRF for each exciting frequency f_i with Direct method. Eq. (2) shows the expression to



Fig. 10. Test setup.



(a) Comparisons of the composite experimental dispersion curve,
 (b) Shear the compacted experimental dispersion curve, and the theoretical dispersion curve determined from the SASW array

Fig. 11. Using the SASW testing to develop the shear wave velocity profile of soil.

calculated \overline{FRF} for each exciting frequency f_i with Average method.

$$FRF_{f_i} = 20 \times \log_{10} \left(\frac{\left| A_{f_i}(t) \right|_{\max,back}}{\left| A_{f_i}(t) \right|_{\max,front}} \right) \tag{1}$$

$$\overline{FRF}_{f_i} = 20 \times \log_{10} \left[\frac{1}{L} \int_0^L \left(\frac{\left| \widehat{A}_{w,f_i}(t, x) \right|_{max}}{\left| \widehat{A}_{wo,f_i}(t, x) \right|_{max}} \right) dx \right]$$
 (2)

where L is 2.44 m, x is the coordinate of sensor measured from the nearest sensor point behind the barrier, $\left|A_{f_i}(t)\right|_{\max,back}$ is the absolute value of maximum acceleration record at the immediate point behind

the barrier, and $\left|A_{f_i}(t)\right|_{\max,front}$ is the absolute value of maximum acceleration record at the immediate point in front of the barrier. $\left|\widehat{A}_{w,f_i}(t,x)\right|_{\max}$ is the maximum normalized ground surface response of the sensor located at sensor location x in the presence of the wave barriers, and $\left|\widehat{A}_{wo,f_i}(t,x)\right|_{\max}$ is the maximum normalized ground surface response of the sensor located at sensor location x without the wave barrier.

When the frequency sweeping excitation or earthquake excitation is applied, the response is transformed to frequency domain by Fast Fourier Transform (FFT). Eq. (3) shows expression to calculated FRF with Direct method. Eq. (4) shows the expression to calculated \overline{FRF} with Average method.

$$FRF(f) = 20 \times \log_{10} \left(\frac{|A(f)|_{back}}{|A(f)|_{front}} \right)$$
(3)

$$\overline{FRF}(f) = 20 \times \log_{10} \left[\frac{1}{L} \int_0^L \left(\frac{\left| \widehat{A}_w(f, x) \right|}{\left| \widehat{A}_{wo}(f, x) \right|} \right) dx \right]$$
 (4)

where L is 2.44 m, x is the coordinate of sensor measured from the nearest sensor point behind the barrier, $|A(f)|_{back}$ is the ground surface response in the frequency domain at the nearest sensor point behind the barrier (Point No. 6 in Fig. 3), and $|A(f)|_{front}$ is the ground surface response in the frequency domain at the nearest sensor point in front of the barrier (Point No. 1 for case B2 and Point No. 5 for cases EL, B1, and BL). $|\widehat{A}_w(f,x)|$ is the normalized ground surface response at the sensor location x in the frequency domain with the presence of the wave barriers, and $|\widehat{A}_{wo}(f,x)|$ is the normalized ground surface response at sensor location x in frequency domain without the wave barrier.

Nine different seismograms are used as the input signals in earthquake excitation and final *FRF* is obtained by averaging the *FRF* results from all nine earthquakes.

The advantage of using the Direct method is that the response of the points in the front and the back of the barriers can be directly compared without normalization. Yet, the performance of the barriers can only be identified by comparing the FRF between the case with barriers and the benchmark case. When the FRF is smaller in the case with the barriers than the case without the barrier, the attenuation is recognized. On the contrary, when the FRF in the case with the barriers is higher than the case without the barrier, the amplification is recognized. While the calculation using Average method incorporates the response of the case with barrier and benchmark case in one expression, the response normalization is necessary, so the resulting FRF is calculated based on the normalized response. Since the normalized response of the benchmark case is used in the denominator for calculating the FRF in Average method, the FRF of benchmark case is a constant 0 by Average method. When the FRF calculated by Average method is below 0, the response reduction is recognized. The advantage of the Average method is that its value of the resulting FRF for the case with barriers is directly related to the amount of response reduction. Moreover, unlike the Direct method only considers the response at two sensor points (one in the front of the barrier, and the other at the back of the barrier) to assess the performance of the barrier, the Average method takes the average of several sensor points within an extended region behind the barrier. The Direct method is expected to show a local effect and the Average method is expected to show a global effect of the presence of the barrier.

3. Experimental results

Except for the existence of the barriers, all the tests are conducted with the same sensors and shaker layout. Three different excitation input

signals and those excitations are applied in the vertical, horizontal crossline, or horizontal inline directions. The three excitation input signals include 1) fix-frequency harmonic excitation, 2) frequency sweeping excitation, and 3) earthquake excitation. The ground surface response is recorded at each sensor location for all three directions. The response in the direction different from the loading direction is not discussed in this paper.

3.1. Normalized response behind the barrier

The normalized ground surface response behind the barrier due to the fix-frequency harmonic excitation is reported in this section. At each loading event, fix-frequency harmonic excitation sends the signal with a constant frequency and amplitude. The 18 frequencies used in fixfrequency harmonic excitation range from 15 Hz to 100 Hz with a 5 Hz interval. This type of excitation is capable of providing concentrated energy at an individual frequency with a high signal-to-noise ratio. Within the 2 s duration, the maximum steady-state response at each sensor location is collected for each exciting frequency. To display the screening effectiveness of the barriers, the ground surface response for all four barrier conditions should be compared with the benchmark case. However, even when the shaker receives an identical input signal, the vibration generated by the shaker is slightly different in its magnitude. Therefore, the response of different barrier conditions cannot be compared directly without normalizing. Dividing the response by the response at the reference point, the normalized response is obtained. The normalized response at the reference point is always one as a result. Located between the vibration source and barrier, the reference point is the nearest point in front of the barrier. In this study, for cases when there is one barrier (i.e. EL, BL, and B1), Point No. 5 is the reference point; for case when there are two barriers (i.e. B2), Point No. 1 is the reference point.

When the excitation is applied in the form of fix-frequency harmonic excitation in any of the three directions, the ground surface responses in the exciting direction are recorded at all the sensor locations behind the barriers. Fig. 12 shows few results of the normalized maximum response at points behind the barrier under fix-frequency harmonic excitation. For the case without the barriers, S0, the ground surface response generally decays as the distance from the vibration source increases due to the geometric decay. However, by observing the response in the benchmark cases shown in Fig. 12, it can be easily realized that the geometric decay is not always followed as the distance increases and the exciting direction has a significant impact on the ground surface response. The ground surface response recorded on the site for the case of SO represents the site characteristics at each exciting frequency. Empty trench (EL) is expected to have the best screening effectiveness since the air cannot transmit the elastic wave, but the response presented in Fig. 12 (d) shows that the EL does not always result in the smallest response among all barrier conditions (BL, B1, B2). The periodic barrier is expected to be more effective when the number of barriers increases. Shown in Fig. 12 (a) and (b), the response is less for the case of B2 than the case of B1. However, the length of the barrier plays an important role in determining its screening effectiveness as well, which can be found by comparing the cases of BL and B1 in Fig. 12 (c) and (d).

3.2. Response in the front and the back of the barrier

Frequency sweeping excitation and earthquake excitation provide a quick way to identify the characteristics of all the barrier conditions within the frequency range of interest (15–100 Hz). The signal for the frequency sweeping excitation introduces a continuous series of sine waves sweeping from 100 Hz to 15 Hz within the duration of 12 s. The response at the most critical locations is displayed to demonstrate the effect of the barrier. These sensor points are the nearest points in the front and at the back of the designated barriers location. For the benchmark case (S0), the response comparison between these two points

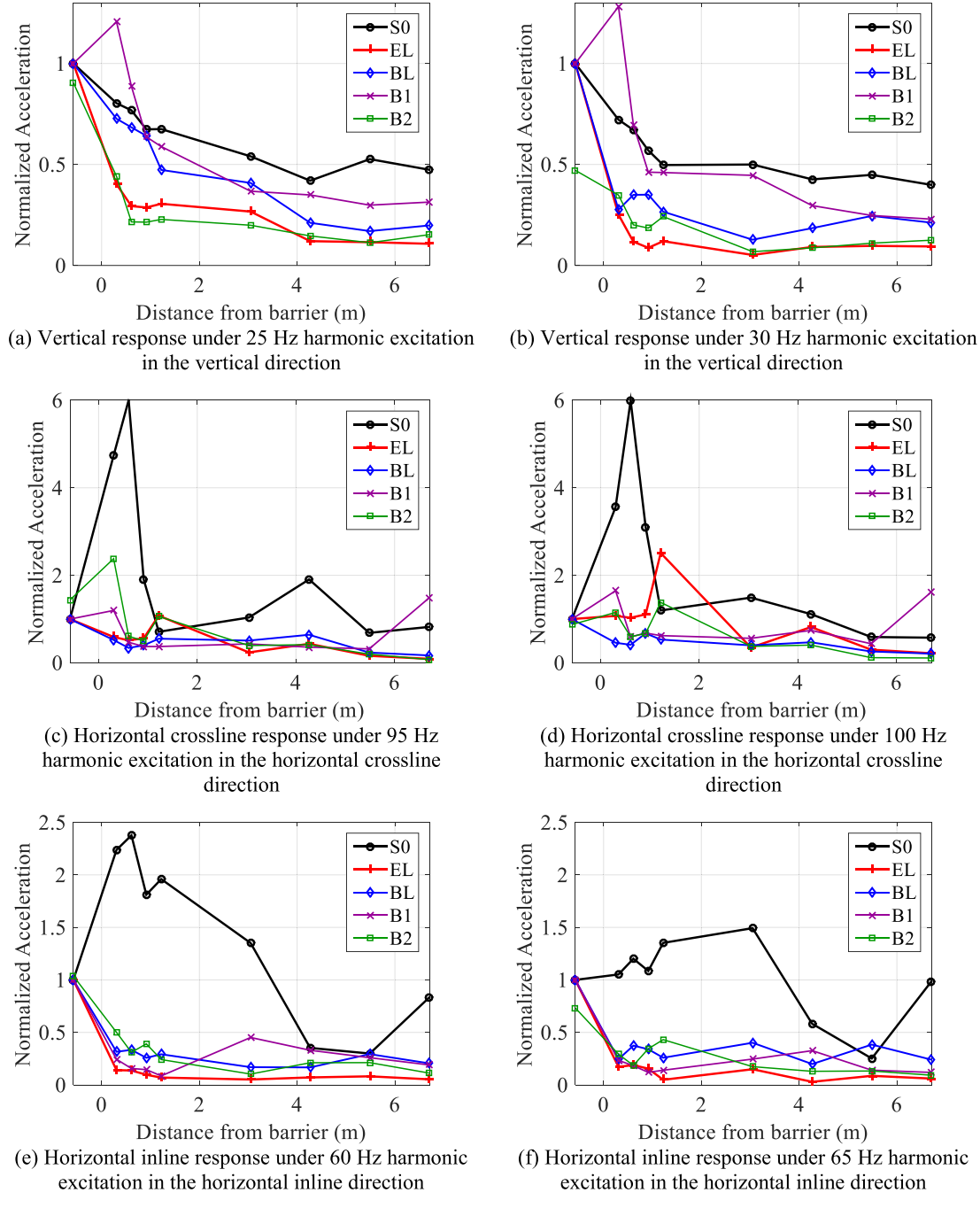


Fig. 12. Normalized maximum response at points behind the barrier under fix-frequency harmonic excitation (black: S0, red: EL, blue: BL, purple: B1, green: B2). (For interpretation of the references to colour in this figure legend, the reader is referred to the Web version of this article.)

reveals the characteristics of the test site. Presented in both time domain and frequency domain, the ground surface response in the front and at the back of the barriers shown in Fig. 13, Fig. 14, and Fig. 15 to stress the importance of exciting frequency to the screening effectiveness of the barriers.

The ground surface response for the case of S0 is presented as a benchmark. Smaller ground surface response is generally observed as the wave propagating away from the vibration source, which is called the geometric decay. It is expected that the ground surface response further reduces with the presence of the barriers in addition to the geometric decay observed in the benchmark case.

Fig. 13 shows the vertical response at nearest points to the front and back of the barriers when vertical excitation is applied. By comparing Fig. 13 (b) and (d), large differences in response reduction are found

within the frequency range of 20–40 Hz and 65–80 Hz in case EL than in case S0. By comparing Fig. 13 (b) and (f), larger differences in response reduction are found within the frequency range of 20–55 Hz and 85–100 Hz in case BL than in case S0. However, unlike the response amplitude decreasing from Point No. 5 to Point No. 6 within 55–70 Hz in case S0, the response amplitude increases from Point No. 5 to Point No. 6 within that frequency range in case BL, which indicates that the existence of the barrier does not offer the vibration isolation but results in a larger response instead. This response amplification may also indicate that the frequency range of 55–70 Hz is within the frequency passband of the metamaterial. By comparing Fig. 13 (b) and (h), the response reduction in case B1 is observed within 60–80 Hz. By comparing Fig. 13 (b) and (j), when Point No.1 and Point No.6 are compared, the response reduction in case B2 is less than in case S0 within 60–100 Hz. Therefore,

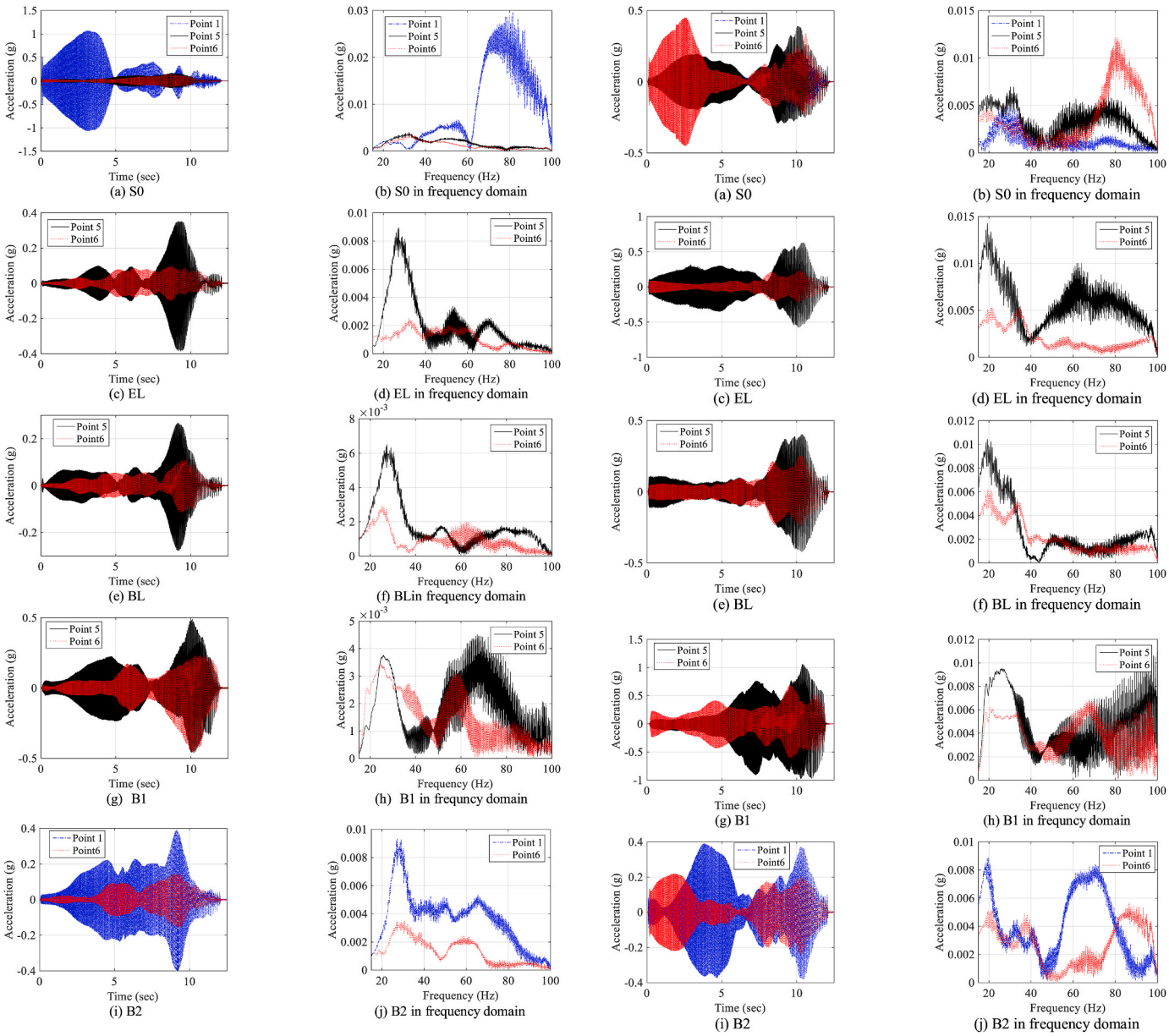


Fig. 13. Vertical response at the points before and after the barrier under vertical frequency sweeping excitation.

even though the response seems to reduce a lot from Point No.1 to Point No. 6 in case B2, the barriers do not provide a good vibration isolation within the frequency range of 60–100 Hz, which may be its frequency passband.

Fig. 14 shows the horizontal crossline response at points nearest to the front and the back of the barriers when the horizontal crossline excitation is applied. As shown in Fig. 14 (b), the response ranging from 70 to 100 Hz at point No. 6 is notably higher than that of Point No. 5 in case S0, and the response at Point No.5 is larger than the response at Point No.1 within the same frequency range. This shows that when there is no barrier, the response amplitude increases as the distance from the vibration source increases within 70–100 Hz. By comparing Fig. 14 (b) and (d), the amount of response amplitude decreases from Point No. 5 to Point No. 6 in case EL and is significantly larger than the amount of amplitude decrease in case S0 within 15–35 Hz and 45–100 Hz. Since the response actually increases from Point No.5 to Point No.6 within 70–100 Hz in case S0 which is shown in Fig. 14 (b), a slight reduction found in case BL shown in Fig. 14 (f) in the same frequency range suggests a huge response reduction due to the periodic barrier within

Fig. 14. Horizontal crossline response at the points before and after the barrier under horizontal crossline frequency sweeping excitation.

70–100 Hz. By comparing Fig. 14 (b) and (h), case B1 displays very good screening effectiveness within 70–100 Hz. By comparing Fig. 14 (b) and (j), when the horizontal crossline excitation is applied, case B2 displays very good screening effectiveness within nearly the entire frequency range of interest.

Fig. 15 shows the horizontal inline response at the nearest points in the front and back of the barrier when the horizontal inline excitation is applied. When the horizontal inline excitation is applied, the response between Point No.1 is much larger than the other two points plotted in Fig. 15 (b) with a different order of magnitude. By comparing the response reduction between Point No.5 and Point No.6 in Fig. 15 (b) and Fig. 15 (d), case EL is showing an excellent response reduction within 15–25 Hz and 35–100 Hz. As shown in Fig. 15 (f), there isn't much difference in the response amplitude at Point No.5 and Point No.6 in Case BL, so the performance of the BL cannot be clearly identified. By comparing Fig. 15 (b) and Fig. 15 (d), the response reduction is seen within 30–70Hz. For Case B2, even though the response reduction is clearly seen between Point No.1 and Point No.6 in Fig. 15 (h), the

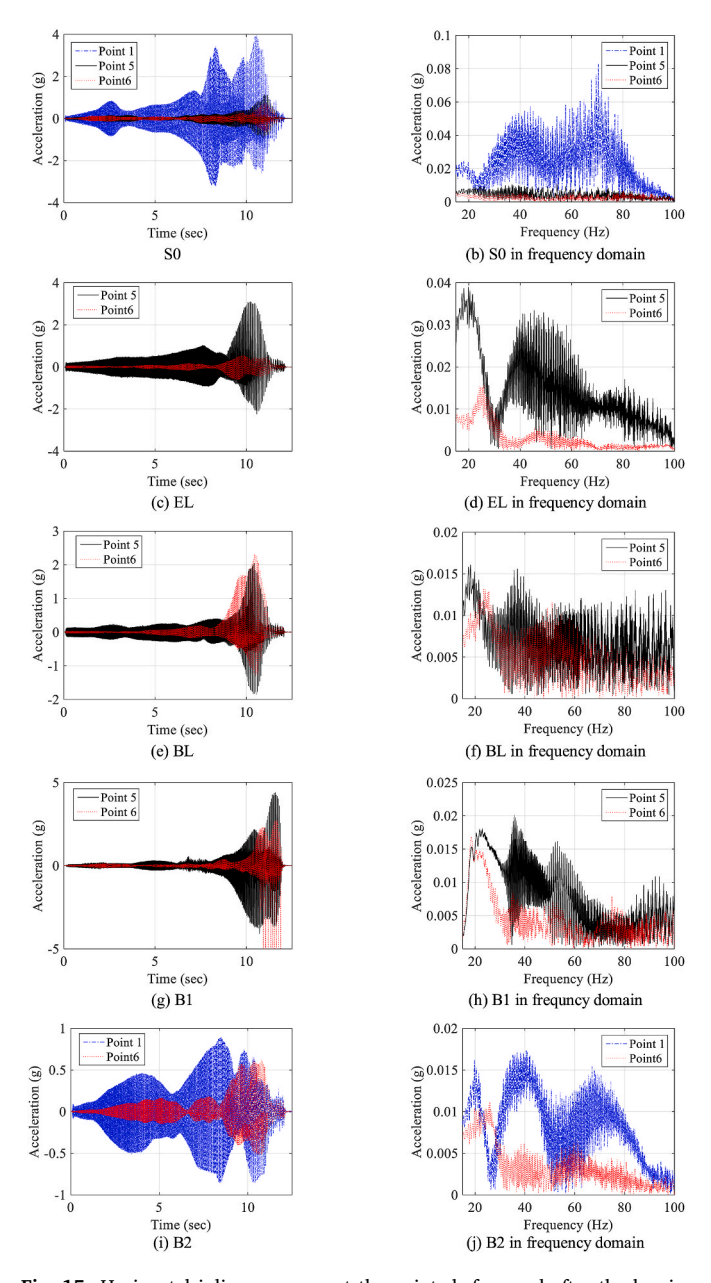


Fig. 15. Horizontal inline response at the points before and after the barrier under horizontal inline frequency sweeping excitation. (Note: The black line represents the response at the point No. 5; the blue line represents the response at the point No. 1; the red line represents the response

represents the response at the point No. 1; the red line represents the response at the point No. 6; the nomenclature of all barrier conditions is mentioned in Sect. 2.3.)

response reduction between these two points in Case S0 is much larger, so the performance of B2 is difficult to identify based on only Fig. 15 (b) and (h).

The influence of the exciting direction on the performance of the barriers is also recognized by comparing Figs. 13, 14, and 15 that the attenuation due to the presence of the barrier is observed in a different frequency range.

3.3. Frequency response function

As defined in Sect.2.5, *FRF* is used to quantify the screening effectiveness of the barriers. Two methods are used to calculate the *FRF*: "Direct method" and "Average method". The Direct method considers response of two sensor points, one in the front and the other at the back

of the barrier, to represent the behavior of the barrier system. Since it takes only two nearest sensor points to the barriers to evaluate the barriers' effectiveness, a local effect of the existence of barriers is revealed from the results of Direct method. Average method takes the average over a certain measuring extent behind the barrier, so it presents the results with global effect of the barriers.

Direct method calculates the *FRF* for each barrier condition (i.e. EL, B1, B2, or BL) and benchmark case (i.e. S0) separately. The resulting *FRF* of the benchmark case represents the characteristics of the site and severs as the threshold to identify the attenuation zones induced by the barrier. When the *FRF* is below the *FRF* of benchmark case, the response reduction is recognized; on the other hand, when the *FRF* is higher than the *FRF* of benchmark case, it means the ground surface response amplifies after the barrier installation.

Figs. 17-20 are the *FRF* results obtained using Direct method. With Point No. 5 as the reference point in the front of the barrier, and Point No. 6 as the point at the back of the barrier, the resulting *FRF* for cases S0, EL, B1, and BL are shown in Figs. 16-18.

Under the vertical excitation, Fig. 16 shows the *FRF* results of vertical response for cases with barrier (EL, B1, BL) and the benchmark case (S0). Fig. 16 (a) shows the results when excitation input signal is in the form of fix-frequency harmonic wave; Fig. 16 (b) shows the results when frequency sweeping is used as the input signal; Fig. 16 (c) shows the results when earthquake seismograms are used as the input signal. comparing the response at Point No. 5 and Point No. 6 for the cases without the barrier (i.e. S0) and with a barrier (i.e. EL, B1, and BL), the wave isolation contributed by the barrier (either EL, B1, or BL) is recognized in some frequency ranges as the resulting *FRF* is lower than the benchmark case, S0.

As shown in Fig. 16 (b) and (c), the FRF results obtained from the excitation input signal of frequency sweeping excitation and earthquake excitation contain the noise of the signal. Using the smooth tool in MATLAB, local regression using weighed linear least squares and a 2nd degree polynomial model is applied. As shown in Fig. 16(d) and (e), the smoothened results exhibit the same characteristics as the results before smoothing. The remaining test results in this section will be presented with this regression technique for a clear presentation.

Based on the different form of input signal, the data is processed differently. The maximum steady state response is extracted from the response when fix-frequency harmonic excitation is used to calculate the FRF; the response is transformed from time-domain to frequency domain for calculating FRF within the entire frequency range (15–100 Hz) when frequency sweeping or earthquake excitation is used; the result obtained from nine earthquakes are averaged when earthquake excitation is used. Yet, as observed from Fig. 16, for all three different excitation input signals, the results are very similar, indicating the reliability of the methodology including the execution of the experiment and the approaches to calculate the FRF. When the excitation is applied in the vertical direction, the following observations are drawn 1) the amplification is found to be in the frequency range of 15-20 Hz and 40-65 Hz for the case of EL, 2) the response reduction is recognized within the frequency range of 65-80 Hz and 90-100 Hz for the case of B1, and 3) the attenuation is achieved except for the frequency range of 60-70 Hz for the case of BL. The FRF resulting from the excitation applied in the horizontal crossline and horizontal inline directions are shown in Figs. 17 and 18 respectively. When the excitation is applied in the horizontal crossline direction, the attenuation due to the barrier occurs within the frequency range of 1) 15–30 and 50–100 Hz for the case of EL, 2) 15-30 Hz and 80-100 Hz for case of B1, and 3) 15-30 Hz and 70-100 Hz for the case of BL. When the excitation is applied in the horizontal inline direction, the attenuation due to the barrier occurs within the frequency range of 1) 15-25 and 35-100 Hz for the case of EL, 2) 30-70 Hz and 90-100 Hz for case of B1, and 3) 30-45 Hz and 55-100 Hz for the case of BL.

The comparison between Figs. 16, 17 and 18 also shows the excitation direction that can lead to an entirely different ground surface

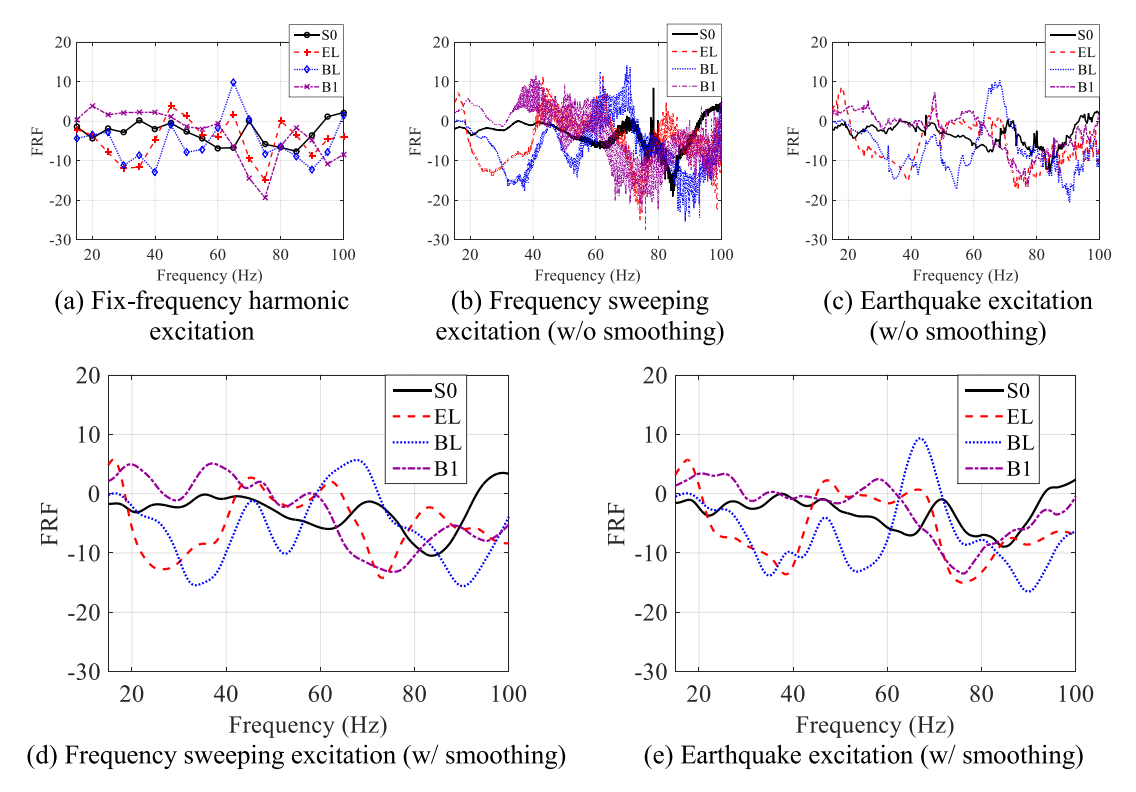


Fig. 16. FRF of vertical response under vertical excitation by Direct method (black: S0, red: EL, purple: B1, blue: BL).. (For interpretation of the references to colour in this figure legend, the reader is referred to the Web version of this article.)

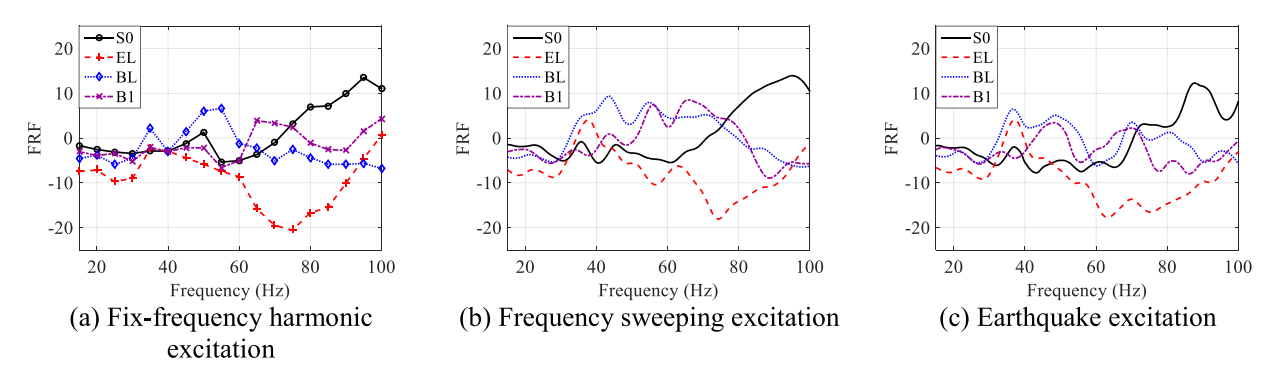


Fig. 17. FRF of horizontal crossline response under horizontal crossline excitation by Direct method (black: S0, red: EL, purple: B1, blue: BL). (For interpretation of the references to colour in this figure legend, the reader is referred to the Web version of this article.)

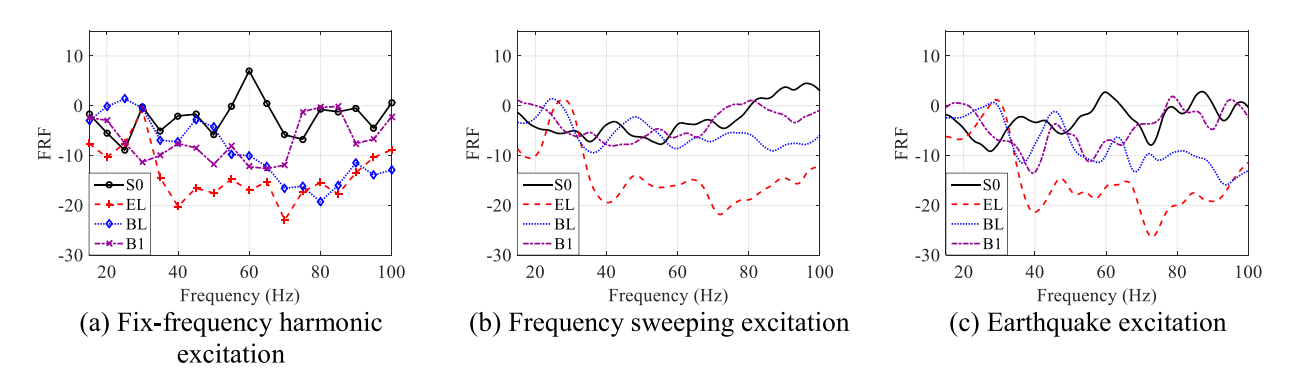


Fig. 18. FRF of horizontal inline response under horizontal inline excitation by Direct method (black: S0, red: EL, purple: B1, blue: BL). (For interpretation of the references to colour in this figure legend, the reader is referred to the Web version of this article.)

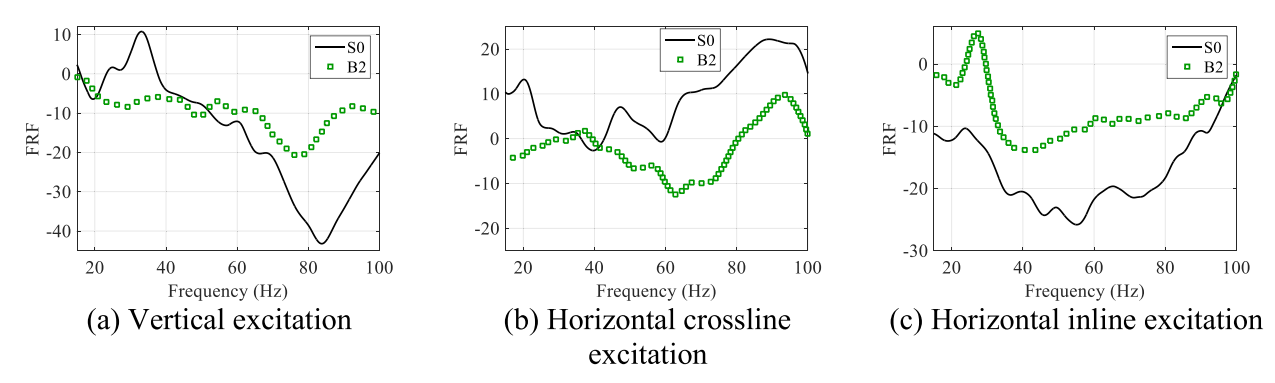


Fig. 19. FRF of ground surface response under frequency sweeping excitation by Direct method (black: S0, green: B2). (For interpretation of the references to colour in this figure legend, the reader is referred to the Web version of this article.)

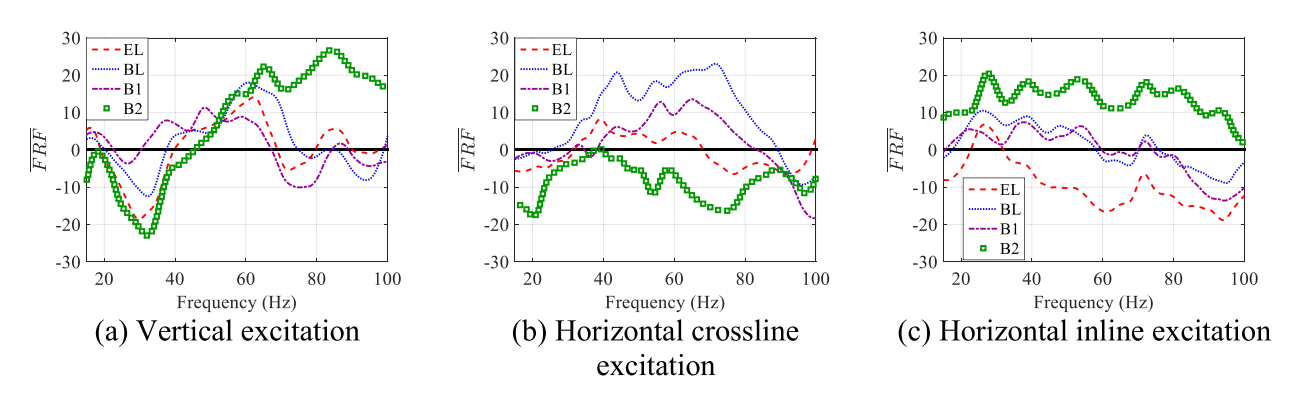


Fig. 20. FRF of ground surface response under frequency sweeping excitation by Average method (black: S0, red: EL, blue: BL, purple: B1, green: B2). (For interpretation of the references to colour in this figure legend, the reader is referred to the Web version of this article.)

response under the same test setup. The effect of the excitation direction is notably significant due to the different dominated wave types generated from the excitation in a different direction. The dominated wave types from vertical excitation, horizontal crossline excitation, and horizontal inline excitation are Rayleigh wave, Love wave, and P wave respectively. The ground surface response attenuation occurring within the frequency band gap of the periodic barrier is recognized from the experimental results.

To evaluate the performance in the case of B2 by Direct method, Point No. 1, located in front of the barriers, is used as the reference point and Point No. 6 is the nearest point at the back of the barriers. From the results shown in Figs. 16–18, it is found that the type of excitation signal does not have much effect on the *FRF* results. Therefore, only the *FRF* results obtained from frequency sweeping excitation is presented in Fig. 19.

The cases of S0 and B2 are compared in Fig. 19 to identify the attenuation zones due to these two short periodic barriers. The attenuation zones due to the two units of barriers occurs within the frequency range of 1) 15–50 Hz under vertical excitation, 2) 15–100 Hz under horizontal crossline excitation. However, when the excitation is applied in horizontal inline direction, the amplification is observed within the frequency range of 15–100 Hz.

Since only two points are considered while calculating the *FRF* with Direct method, the attenuation zones identified through Direct method can vary with the selection of the points representing the front and the back of the barrier. The results may only represent local effects. On the other hand, the Average method takes the response within an extended region into the calculation, so the attenuation zones identified through Average method present a global effect of the presence of barriers. However, based on the test results, the attenuation zones identified from Direct method and Average method shares some resemblance. The

advantage of using Direct method is that it requires as little as two sensors to picture the performance of the barrier, but the local effect may not well represent the whole barrier system. The Average method, on the other hand, reveals the performance of the barriers by the response of a region protected by the barriers. Moreover, since the Average method incorporates the response in the benchmark case in the calculation, the *FRF* value obtained from Average method directly relates to the amount of response reduction. Due to the page limitation, since the results for all three different input signals are showing a good agreement with each other, only the frequency sweeping excitation test results are presented in Fig. 20.

The results from both methods shows certain level of resemblance for cases EL, B1, and B2. However, the attenuation zones identified by the Average method does not match the results from the Direct method for case BI

Excitation direction plays an important role in the performance of the barrier. Even though the characteristics of the barrier are not altered by the excitation direction, the filtering ability of the barrier is highly depending on the type of wave transmitting through the barrier. For example, the frequency band gaps for metamaterial subjected to P wave is different from S wave (while its complete frequency band gaps remain the same). The dominate wave type is determined by the excitation direction, site conditions, and the distance from the vibration to the targeted object. The performance of the barrier is, therefore, dependent on the excitation direction.

The theory of the metamaterial is built on the assumption that the material is infinitely large in its length and depth. While the depth of the barrier is fixed to 1.52 m in this experiment, two different length of the periodic barrier are considered. The effect of the length of the barrier can be found by comparing the results of case BL and B1. It is found having a barrier with longer length does not guarantee to be more

effective. As shown in Fig. 20, depending on the exciting frequency and the excitation direction, the shorter barrier (B1) can display a better performance than the longer barrier (BL). However, by comparing the results of BL and B1 in Table 2, it is found that response reduction due to the long barrier (BL) occurs in a wider frequency range than short barrier (B1) when Direct method is implemented. As Direct method demonstrates the local effect, this observation suggests that the effect of the barrier length is most conspicuous near the barrier.

It is believed that having a larger number of barriers is beneficial to the screening effectiveness of the barrier system, which suggests that when the second barrier is added, the response should be further reduced from the case with one barrier. While the depth in all barrier conditions considered in this experiment are identical, which is 1.52 m. The effect of the number of barriers can be found by comparing the results of case B1 and B2. Observed from Fig. 20 (b), when excitation is applied in horizontal crossline direction, the performance of two periodic barrier is apparently better than one periodic barrier. While the attenuation zones are found to be 15-30 Hz and 85-100 Hz for case B1. the attenuation zone for case B2 is widened to cover the entire frequency range of interest (15–100 Hz). However, as shown in Fig. 20 (a) and (c), have two barriers does not guarantee to have better screening effectiveness. The performance of case B1 is better than case B2 within the frequency range of 55-100 Hz under vertical excitation, and 15-100 Hz under horizontal inline excitation. The reason could be that the separation between the two barriers is too long to exclude the effect of the soil.

4. Conclusions

Under our experimental program, four barrier conditions: EL (empty trench), BL (long periodic barrier), B1 (one short periodic barrier), and B2 (two short periodic barriers) are studied. For each barrier condition, three different excitation input signals are applied in all three directions, and the ground surface response is recorded in all three directions. Along with these four barrier conditions, the benchmark case, S0, is tested prior to the barrier installation. The following conclusions are drawn from the experiments:

- 1. The three different excitation input signals—fix-frequency excitation, frequency sweeping excitation, and earthquake excitation—yield similar results. This shows the methodology of conducting the field test is reliable that the vibration can be generated and very well controlled by the shaker. The shaker can generate the requested signal and in lieu of the input signal. Moreover, since different approach is used to process the data subjected to different form of input signal, having the results highly agree with each other shows the way the data is processed is also reliable.
- 2. Direct method demonstrates a local effect of the barriers while Average method shows a global effect. The advantage of Direct

Table 2Attenuation zones identified from Direct method and Average method.

Excitation Direction	Barrier condition	Direct method (Hz)	Average method (Hz)
Vertical	EL	20-40,70-80,90- 100	20-40,70-80
	BL	15-55,75-100	20-40,80-100
	B1	65-80,90-100	20-25,65-100
	B2	15-50	15-50
Horizontal	EL	15-30,50-100	15-30,65-100
Crossline	BL	15-30,70-100	15-20,90-100
	B1	15-30,80-100	15-30,85-100
	B2	15-100	15-100
Horizontal Inline	EL	15-20,30-100	15-20,35-100
	BL	30-45,55-100	60-70,75-100
	B1	30-70,90-100	75–100
	B2	None	None

method is that it requires as few as two sensor points to evaluate the barrier performance, and its disadvantage is that the results is only meaningful when it is compared with the result from benchmark case. The advantage of Average method is that its *FRF* value is directly related to the amount of response reduction since it had incorporate the result of benchmark case in its calculation, and its disadvantage is that it requires more sensor to capture the response in the region behind the barriers. Interestingly, the results from both methods shows certain degree of resemblance for case EL, B1, and B2. However, the attenuation zones identified by the Average method does not match the results from the Direct method for case BL.

- 3. From the Direct method, the performance of the barriers is recognized by comparing the *FRF* results between the benchmark case (S0) and case with barriers (EL, BL, B1, or B2). The *FRF* of the benchmark case demonstrates the characteristics of the site, which shows the response of the site with absence of the barriers. By observing the *FRF* results from the case of S0, it is found the soil responds much differently as the excitation direction is switched implying the different dominate wave types are presented.
- 4. The excitation direction has a major impact on the performance of the barriers due to the different dominated wave types generated from the excitation in a different direction. The dominate wave type is determined by the excitation direction, site conditions, and the distance from the vibration to the targeted object. The performance of the periodic barrier is highly dependent on the type of wave transmitting through the periodic barrier. In addition, the excitation direction also makes a difference in the amount of the reflection from the next soil layer or from the edge of the site. Therefore, the performance is highly dependent on the excitation direction.
- 5. The effect of the infilled material is studied by comparing the empty trench (EL) and periodic barrier (BL) with the same dimension. The empty trench was expected to be the most effective type of barrier to screen the vibration. However, it is found the performance of both EL and BL is highly dependent on the exciting frequency and excitation directions. Therefore, the case of BL can outperform the case of EL in some frequency ranges while subjected to the excitation in certain direction.
- 6. The effect of barrier length is studied by comparing the one short periodic barrier (B1) and one long periodic barrier (BL). The benefit of longer barrier length on the performance of the barrier is found to be more conspicuous near the barrier. This local effect can be observed from the result of Direct method.
- 7. The effect of the number of barriers is studied by comparing the one short periodic barrier (B1) and two short periodic barriers (B2). Each of the barrier unit has identical dimension. However, it is found that two barriers do not always to have better screening effectiveness than one barrier. The reason could be that the separation between the two barriers is too long to exclude the effect of the soil.
- 8. The frequency band gap is the characteristic that the metamaterial possesses. When the wave with the frequency falls within the frequency band gap, wave propagation is prohibited through the material. The attenuation attributed to the metamaterial barriers is observed in certain frequency ranges in the experiments, and those frequency ranges are significantly affected by the excitation direction.

CRediT authorship contribution statement

Hsuan Wen Huang: Field test, Writing - original draft, Writing - review & editing, Methodology, Visualization. Benchen Zhang: Field test, Investigation, Validation, Data curation. Jiaji Wang: Writing - original draft, Writing - review & editing, Methodology, Formal analysis, Visualization. F.-Y. Menq: Writing - review & editing, Field test, Data curation, Resources. Kalyana Babu Nakshatrala: Writing - review & editing, Methodology, Validation, Supervision. Y.L. Mo: Writing -

review & editing, Resources, Supervision, Project administration, Funding acquisition. **K.H. Stokoe:** Writing - review & editing, Resources, Supervision, Project administration, Funding acquisition.

Declaration of competing interest

The authors declare that they have no known competing financial interests or personal relationships that could have appeared to influence the work reported in this paper.

Acknowledgments

This study is financially supported by the National Science Foundation under grant 1761659. The authors would like to express gratitude to NHERI@UTexas for the experiment execution.

References

- Gao G, Li N, Gu X. Field experiment and numerical study on active vibration isolation by horizontal blocks in layered ground under vertical loading. Soil Dynam Earthq Eng 2015;69:251–61.
- [2] Wang J-G, Sun W, Anand S. Numerical investigation on active isolation of ground shock by soft porous layers. J Sound Vib 2009;321:492–509.
- [3] Gao G, Li Z, Qiu C, Yue Z. Three-dimensional analysis of rows of piles as passive barriers for ground vibration isolation. Soil Dynam Earthq Eng 2006;26:1015–27.
- [4] Liao S, Sangrey DA. Use of piles as isolation barriers. J Geotech Geoenviron Eng
- [5] Woods RD. Screening of surface waves in soils. In: Industry program of the colledge of engineering. The University of Michigan; 1968.
- [6] Coulier P, Hunt HE. Experimental study of a stiff wave barrier in gelatine. Soil Dynam Earthq Eng 2014;66:459–63.
- [7] Xu L. Influence of in-filled trench as wave barrier on ground vibrations. 2012.
- [8] Çelebi E, Fırat S, Beyhan G, Çankaya İ, Vural İ, Kırtel O. Field experiments on wave propagation and vibration isolation by using wave barriers. Soil Dynam Earthq Eng 2009;29:824–33.
- [9] Alzawi A, El Naggar MH. Full scale experimental study on vibration scattering using open and in-filled (GeoFoam) wave barriers. Soil Dynam Earthq Eng 2011; 31:306–17.
- [10] Ulgen D, Toygar O. Screening effectiveness of open and in-filled wave barriers: a full-scale experimental study. Construct Build Mater 2015;86:12–20.
- [11] Coulier P, Cuéllar V, Degrande G, Lombaert G. Experimental and numerical evaluation of the effectiveness of a stiff wave barrier in the soil. Soil Dynam Earthq Eng 2015;77:238–53.

- [12] Witarto Witarto, Nakshatrala Kalyana B, Mo YL. Global sensitivity analysis of frequency band gaps in one-dimensional phononic crystals. Mech Mater 2019;134: 38–53. In press, https://doi.org/10.1016/j.mechmat.2019.04.005.
- [13] Huang Hsuan Wen, Wang Jiaji, Zhao Chunfeng, Mo Yi-Lung. Two-dimensional finite-element simulation of periodic barriers. ASCE J Eng Mech 2021;147(2): 04020150. In press, https://doi.org/10.1061/(ASCE)EM.1943-7889.0001891.
- [14] Huang Hsuan Wen. Periodic Metamaterial-Based Seismic Isolation Barriers: Field Stuties and Computational Modeling. PhD thesis. Houston, TX: University of Houston, Department of Civil and Environmental Engineering; 2020. In press.
- [15] Huang J, Shi Z, Huang W, Chen X, Zhang Z. A periodic foundation with rotational oscillators for extremely low-frequency seismic isolation: analysis and experimental verification. Smart Mater Struct 2017;26:035061.
- [16] Xiang H, Shi Z, Wang S, Mo Y. Periodic materials-based vibration attenuation in layered foundations: experimental validation. Smart Mater Struct 2012;21:112003.
- [17] Witarto W, Wang S, Yang C, Nie X, Mo YL, Chang K, et al. Seismic isolation of small modular reactors using metamaterials. AIP Adv 2018;8:045307.
- [18] Witarto W, Wang S, Yang C, Wang J, Mo Y, Chang K, Tang Y. Three-dimensional periodic materials as seismic base isolator for nuclear infrastructure. AIP Adv 2019; 9:045014.
- [19] Yan Y, Laskar A, Cheng Z, Menq F, Tang Y, Mo Y, Shi Z. Seismic isolation of two dimensional periodic foundations. J Appl Phys 2014;116:044908.
- [20] Yan Y, Cheng Z, Menq F, Mo Y, Tang Y, Shi Z. Three dimensional periodic foundations for base seismic isolation. Smart Mater Struct 2015;24:075006.
- [21] Meseguer F, Holgado M, Caballero D, Benaches N, Sanchez-Dehesa J, López C, Llinares J. Rayleigh-wave attenuation by a semi-infinite two-dimensional elasticband-gap crystal. Phys Rev B 1999;59:12169.
- [22] Brûlé S, Javelaud E, Enoch S, Guenneau S. Experiments on seismic metamaterials: molding surface waves. Phys Rev Lett 2014;112:133901.
- [23] Pu X, Shi Z. Periodic pile barriers for Rayleigh wave isolation in a poroelastic halfspace. Soil Dynam Earthq Eng 2019;121:75–86.
- [24] Brûlé S, Enoch S, Guenneau S. Experimental evidence of auxetic features in seismic metamaterials: ellipticity of seismic Rayleigh waves for subsurface architectured ground with holes. 2018. arXiv preprint arXiv:1809.05841.
- [25] Pu X, Shi Z. Broadband surface wave attenuation in periodic trench barriers. J Sound Vib 2020;468:115130.
- [26] Krödel S, Thomé N, Daraio C. Wide band-gap seismic metastructures. Extreme Mechanics Letters 2015:4:111–7.
- [27] Palermo A, Krödel S, Marzani A, Daraio C. Engineered metabarrier as shield from seismic surface waves. Sci Rep 2016;6:39356.
- [28] Zeng Y, Peng P, Du Q-J, Wang Y-S. A novel zero-frequency seismic metamaterial. 2019. arXiv preprint arXiv:1907.06446.
- [29] Witarto W. In: Periodic material-based seismic base isolators for small modular reactors. Texas: Department of Civil and Environmental Engineering, University of Houston: 2018.
- [30] Stokoe K, Cox B, Clayton P, Menq F. NHERI@ UTexas experimental facility: large-scale mobile shakers for natural-hazards field studies. In: 16th world conference on earthquake engineering; 2017. Santiago, Chile.